Scale Invariance of the Stress Production Mechanism in Polymeric Systems

R. C. Picu* and M. C. Pavel

Department of Mechanical, Aerospace and Nuclear Engineering, Rensselaer Polytechnic Institute, Troy, New York 12180

Received December 19, 2002; Revised Manuscript Received September 22, 2003

ABSTRACT: Stress production in a model monodisperse polymeric material is investigated on multiple scales. The analysis is performed by means of equilibrium and nonequilibrium molecular dynamics. A family of mobile intrinsic coordinate systems is introduced, each system having one axis tied to the end-to-end vector of a generic chain segment of specified length. A similar mobile coordinate system tied to the large semiaxis of the ellipsoidal chains is defined on the chain scale. The atomic level stress is evaluated based on bonded and nonbonded interatomic interactions and averaged in the global coordinate system, to result in the global, system level stress, and in the various intrinsic systems, to result in intrinsic stresses. It is observed that the deviatoric intrinsic stress is scale independent, a bond, a chain segment, and the chain scale intrinsic frame carrying the same stress. The hydrostatic component of the stress tensor scales with the segment length. This concept extends the previously introduced intrinsic stress framework, scale linking the bond and chain scales. During melt deformation, the chain segments stretch and rotate. Chains shorter than the entanglement length mainly rotate during an elongational deformation of limited amplitude, their size remaining essentially constant. Longer chains distort and rotate. Two regimes are evidenced during the return to isotropy of the orientation on multiple scales. The faster mode is associated with the return to equilibrium of the internal structure of the generic chain, while the slower mode is associated with chain rotation in the global coordinate system. The intrinsic deviatoric stress carried by a chain changes during the first mode, and is essentially constant during the second. The physical picture of stress production defined on the scale of a bond (Kuhn segment) in the intrinsic stress framework translates to the chain scale during this late relaxation regime: each rotating chain carries a constant deviatoric intrinsic stress, the preferential chain orientation leading to a nonzero global deviatoric stress.

1. Introduction

The mechanism of stress production in polymeric systems has received attention early in the development of the molecular theories of polymer dynamics. The classical description dates back to the work of Guth and Mark[1] who proposed that stress production is associated with the loss of entropy of a chain being stretched. This loss of entropy translates into the variation of the free energy, which then leads to a force and therefore to a material stress. The force acts between the two ends of the chain being stretched and is aligned with the end-to-end vector. The force is always retractive and therefore the chains are always in tension. For small deformations, the force increment is proportional to the stretch. Furthermore, the force is proportional to the absolute temperature, which is the signature of its entropic nature. The linearity with deformation and the conjectured purely entropic character of the force (and associated stress) led to regarding the chains as "entropic springs in tension."

The energetic component of the free energy is usually neglected in this theory. This is based on the conjecture that the neighborhood of a representative chain segment does not change significantly during deformation and does not lead to deviatoric stress production. Therefore, only the average segment orientation and hence the configurational entropy change.

The entropic spring model has been widely used over the past half century. However, a series of experiments and simulations point to limitations of this fundamental concept.[2−4,43,45] The theory applies only to chains that are long enough to behave as Gaussian chains, it does not apply in situations in which the deformation fields change significantly over a length scale comparable with the chain size, and cannot capture fast local processes that take place on the subchain scale (e.g., β relaxation).

Experimental indications exist suggesting that the excluded volume plays a crucial role in stress production. The excluded volume has been introduced in the theory in a number of ways:[5−12] as a mean field contributing to pressure only and therefore preventing the chains from collapsing, in the form of constraining tubes through which chains diffuse, as in the reptation model, through the entanglement and entanglement slip concepts, etc. However, these advances were generally focused on chain dynamics, rather than on stress production.

These observations led to the development of the intrinsic stress framework (ISF) in which stress production is viewed on the atomic scale.[13−25] In this formulation, stress results from the bonded and nonbonded interatomic interactions, while the excluded volume effect is accounted for at all times. The physical picture on which ISF is based is that the steric shielding generates a local deviatoric stress on the bead (representing a Kuhn segment or a monomer) scale, "intrinsic stress" which is essentially independent of the material deformation. The deformation independence condition is fulfilled in the melt up to considerable strains and implies that the neighborhood of a representative bead is largely invariant.

The ISF allowed for some fundamental advances to be made. It was shown that the system level stress evaluated within ISF is entropic, this being an outcome

10.1021/ma0259867 CCC: $25.00
Published on Web 10/25/2003

rather than an assumption of the model, as in the entropic spring theory. The stress−optical coefficient may be evaluated within ISF based on intrinsic stresses which, in turn, are computable from equilibrium simulations. Since ISF is based on the scale of a bond, it is equally applicable to short and to long chains, and can equally account for fast and slow relaxation/deformation modes.

The present work is part of an ongoing effort to develop the new formalism. Here, we develop a generalization of the concept of intrinsic stresses by extending the framework to scales larger than that of the bond, while consistently accounting for the small scale physics. The article is organized as follows: the model, the simulation procedure, the definition of the intrinsic coordinate system, and intrinsic stresses are presented first. Then, the principal concepts of ISF are reviewed. Furthermore, the new results are presented and the ensuing physical insight is discussed. The conclusions are summarized in closure.

2. Model and Simulation Procedure

The model polymers used in this study are of the "pearl necklace" type, or chains of spherical beads. Each bead represents a Kuhn segment. The beads are connected by stiff linear springs represented by a quadratic potential:

$$u_b(r) = \frac{1}{2}\kappa(r - b_0)^2 \tag{1}$$

Here, r denotes the distance between any pair of atoms and b_0 is the undeformed bond length. The spring constant κ has a value corresponding to $(\kappa b_0^2/k_B T) = 267$, while $b_0 = 1$. The springs are stiff enough to prevent chain crossing. The system is monodisperse with the chains containing $N = 11$, 21, 41, 61, and 101 beads each, in separate simulations.

Beads not directly connected along a chain interact through nonbonded interactions described by a purely repulsive 12−6 Lennard-Jones potential. Nonbonded interactions between beads of different chains (inter) as well as between not covalently connected beads of the same chain (intra) are considered. The cutoff radius of the potential is defined by $R_c = 2^{1/6}\sigma_{LJ}$. No bending or torsional potentials were used, the bonds being free to rotate in the limit of the excluded volume constraint. The Lennard-Jones potential defines the units of the problem, with the length scale σ_{LJ} and the energy ϵ_{LJ} in the potential defining the units of length and energy, and $\sigma_{LJ}\sqrt{m_0/\epsilon_{LJ}}$ and $\epsilon_{LJ}/\sigma_{LJ}^3$ being the units for time and stress, respectively.

The simulation cell is cubic in equilibrium, with the size L defined by the imposed number density of the system $\rho = (NN_c\sigma_{LJ}^3/L^3)$. Here N_c represents the number of chains in a given simulation. Periodic boundary conditions are used as customary in molecular dynamics. Dense melts were considered in all simulations discussed here, with $\rho = 1$ and $T = 1.2$. The total number of beads in a model was about 3000, while the number of chains varied from $N_c = 18$ to 140 in various simulations, depending on the chain length N.

The initial configuration of the system of chains is obtained by performing self-avoiding random walks on a dummy bcc lattice that fills the undeformed simulation cell. The lattice self-avoiding walk is not an efficient chain generating algorithm at high densities due to the high probability of overlaps. To avoid such problems, a modified procedure by which a virtual energetic cost is associated with each overlap (which are therefore permitted during system generation) is used in conjunction with a Monte Carlo generation algorithm. Once the system is constructed, the chains are evolved on the lattice by performing a combination of reptation and crankshaft MC moves until all overlaps are eliminated. The procedure is described in.[26] Further, a high-temperature equilibration is performed by molecular dynamics, to obtain a proper melt structure.

The algorithm and the thermostat proposed by Berendsen et al.[27] are used to integrate the equations of motion. The parameter Ω in the algorithm, which controls the speed of response of the thermostat to a temperature perturbation, is taken to be $\Omega = 10\Delta t$. For this value it was verified that in nonequilibrium simulations the temperature at the onset of relaxation is the target temperature and remains so throughout the relaxation. The Berendsen algorithm is fast responding and accurately maintains the setup system temperature even under high strain rate-high energy input conditions. The time step of integration Δt is kept constant for the whole loading-relaxation period and equal to 0.001.

In simulations performed under nonequilibrium conditions, the melt deformation is induced by a volume-preserving elongational deformation of the unit cell. The deformation of the interior of the cell is imposed through the boundary conditions. During such a deformation, with the stretch direction x_1, the cell size is modified according to

$$L_1 = L(1 + \dot{\epsilon}t)$$
$$L_2 = L/(1 + \dot{\epsilon}t)^{1/2}$$
$$L_3 = L/(1 + \dot{\epsilon}t)^{1/2} \tag{2}$$

where $\dot{\epsilon}$ is the strain rate. All simulations reported here were performed with a strain rate $\dot{\epsilon} = 0.1$ and the total deformation of the cell in the stretch direction is 20% (the stretch, λ, is $\lambda = 1 + \dot{\epsilon}t_{loading} = 1.2$). The melt was deformed up to 50% in several simulations. The periodic boundary conditions remain unchanged during deformation.

The results were obtained by averaging over a large number of replicas (400 replicas for systems in nonequilibrium) in order to reduce the statistical noise.

3. Definition of Intrinsic Frames and Stress Evaluation

Several coordinate systems associated with various entities of the chain on various scales are defined in Figure 1. The global coordinate system x_i associated with the simulation cell (the laboratory frame) is also shown. The system labeled "bond-intrinsic" in Figure 1 is the bond scale intrinsic coordinate system of the intrinsic stress framework.[13,22] It has one of its axes, $\tilde{x}_1$, tied to the bond connecting two adjacent beads. Hence, the frame is mobile, rotating along with the bond. A similar frame tied to the end-to-end vector of a subchain segment composed of N^{seg} bonds is also defined. This forms a family of mobile segment-intrinsic frames that rotate with the respective segment, with N^{seg} changing from 5 to the total number of bonds in the chain, $N - 1$.

A tilda, $\tilde{\ }$, over each quantity shows that it is evaluated in an intrinsic coordinate system. No additional notation is used for the "bond-intrinsic" system, a "seg" superscript is used for the various "segment-intrinsic" systems, and an "ee" superscript is used for the intrinsic frame tied to the end-to-end vector of the representative chain.

In the bulk, polymer chains have, in average, the shape of a flattened ellipsoid. This shape may be evidenced by computing the gyration tensor[28] defined by

$$G_{ij} = \frac{1}{N}\sum_{k=1}^{N}(X_i^k - X_i^{CM})(X_j^k - X_j^{CM})$$

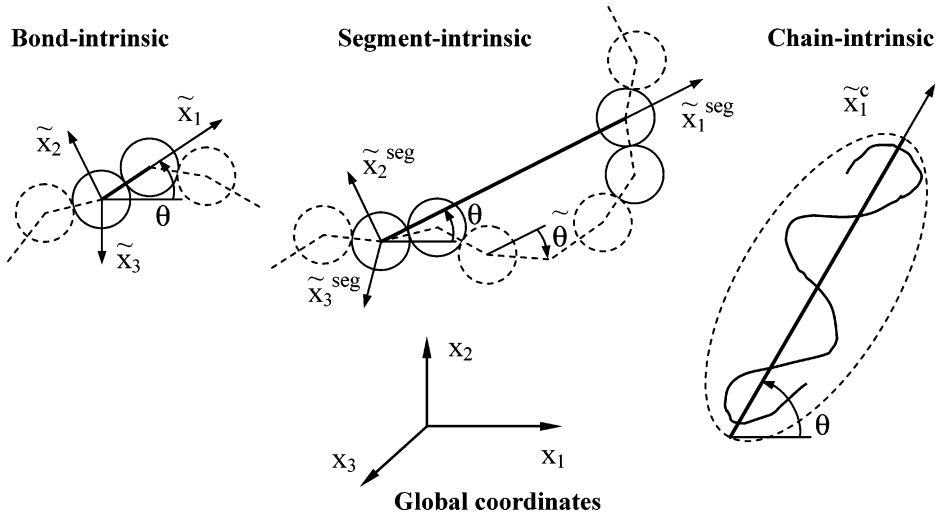

Figure 1. Definition of the bond-, segment-, and chain-intrinsic coordinate systems, as well as of the global coordinate system.

where $\mathbf{X}^k = \{X_1^k, X_2^k, X_3^k\}$ is the position vector of bead k, and CM stands for the center of mass of the current chain. The eigenvalues of the tensor represent the square of the semiaxes of the ellipsoidal chain. The ratio of the three eigenvalues in the present model is 11.7:2.6:1, while the corresponding ratio obtained from a random walk is 12.07:2.72:1.[29] In equilibrium, the large semiaxis (the eigenvector corresponding to the largest eigenvalue) is randomly oriented in space. Here, a "chain-intrinsic" frame is associated with the principal axes of the ellipsoidal chain (Figure 1), with the $\tilde{x}_1$ axis of this frame being tied to the longest semiaxis of the coil. Quantities referring to this coordinate system are denoted by a "c" superscript.

The position of the $\tilde{x}_1$ axis of the various systems with respect to the global x_1 axis is defined by the angle θ, while the orientation of the bonds with respect to the segment and chain-intrinsic $\tilde{x}_1$ axis is defined by $\tilde{\theta}$. The average orientation of the various intrinsic frames with respect to the global coordinates is given by the second moment of the distribution function, the Legendre polynomial

$$\langle P_2(\theta)\rangle = \left\langle \frac{1}{2}(3\cos^2\theta - 1)\right\rangle \tag{3}$$

where the average is taken over all frames and over all replicas of the system.

The orientation of bonds with respect to the segment and chain-intrinsic frames is defined by the same measure computed as a function of $\tilde{\theta}$

$$\langle \tilde{P}_2^{\text{seg}}(\tilde{\theta})\rangle = \left\langle \frac{1}{2}(3\cos^2\tilde{\theta} - 1)\right\rangle \tag{4}$$

where the average is taken over all bonds in the respective segment and over all segments of similar length in the simulation and system replicas.

The orientation is characterized by the second Legendre polynomial because this measure is associated with the birefringence of the system of chains and with the global stress (section 4),[15,22] since its Fourier transform relates directly to NMR measurements.

Stress is computed in the global coordinate system x_i using the virial formula

$$\langle t_{ij}\rangle = \langle t_{ij}^{\text{b}} + t_{ij}^{\text{nb}}\rangle = \frac{1}{v}\Big\langle \sum_{\text{m}\in b} R_{\text{m}}{}^{-1} u'_{\text{b}}(R_{\text{m}}) R_{\text{m}i} R_{\text{m}j}\Big\rangle + \frac{1}{v}\Big\langle \sum_{\text{m}\in \text{nb}} R_{\text{m}}{}^{-1} u'_{\text{nb}}(R_{\text{m}}) R_{\text{m}i} R_{\text{m}j}\Big\rangle \tag{5}$$

where the notation m ∈ b and m ∈ nb indicates that the sums range over all pairs of bonded and nonbonded interacting atoms. The angular parentheses represent averaging over all beads in the system and over all configurations. The volume v corresponds to a bead and is computed as the inverse of the bead number density. u'_{b} and u'_{nb} are the first derivatives of the bonded and nonbonded potentials, respectively, and **R** is the position vector of a neighbor with respect to the representative bead. The kinetic contribution to stress that usually appears in the virial formula is not included in eq 5 since it contributes to pressure only. In the present discussion, we are interested in the deviatoric component of stress

$$\langle {}^{D}\sigma_{ij}\rangle = \langle t_{ij}\rangle - \delta_{ij}\langle t_{kk}\rangle/3 \tag{6}$$

The virial formula is also used to evaluate the atomic level stress, $\langle \tilde{t}_{ij}\rangle$, and its deviatoric component, $\langle {}^{D}\tilde{\sigma}_{ij}\rangle$ (eq 6), in the bond-intrinsic coordinate system. The bond-intrinsic stress results by averaging over all similar frames in the system and over all phase space trajectories

$$\langle \tilde{t}_{ij}\rangle = \langle t_{\text{rs}} a_{\text{ir}} a_{\text{js}}\rangle \tag{7}$$

where a_{ir} are components of the rotation matrix relating the global and bond-intrinsic coordinate systems for the current bead.

The segment and chain-intrinsic stresses are computed in a similar manner by rotating the contribution of a bead from the bond-intrinsic to the segment (chain)-intrinsic system, summing up contributions of all beads belonging to the respective segment, and finally averaging over all segments (chains) in the system:

$$\langle \tilde{t}_{ij}{}^{\text{seg}}\rangle = \Big\langle \sum_{k=1}^{N^{\text{seg}}} \tilde{t}_{\text{rs}}^{k}\, \tilde{a}_{\text{ir}}^{k}\, \tilde{a}_{\text{js}}^{k}\Big\rangle \tag{8}$$

In eq 8, $\tilde{a}_{ir}^{k}$ are components of the rotation matrix relating the bond-intrinsic and segment or chain-intrinsic coordinate systems for bead k of the current segment and $\tilde{t}_{rs}^{k}$ is the bond-intrinsic stress of the same bead. The superscript "seg" may be replaced by "ee" and "c" representing intrinsic stresses in the end-to-end coordinate system and the chain coordinate system (Figure 1), respectively.

The origin of the intrinsic deviatoric stress in the various coordinate systems is identical to that of the global stress, all quantities being evaluated based on the same interatomic interactions.

It is useful to discuss the level of statistical error that affects the computed quantities. The most accurate quantities are those associated with the bond: the bond-intrinsic stresses, $\langle {}^{D}\tilde{\sigma}_{ij}^{b}\rangle$ and $\langle {}^{D}\tilde{\sigma}_{ij}^{nb}\rangle$, and the measure of the preferential bond orientation in global coordinates, $\langle P_2\rangle$. These quantities are evaluated as averages over all bonds in the system and over all replicas (400 replicas). The error bar on the bond-intrinsic stresses is ± 0.025, while that on $\langle P_2\rangle$ is ± 0.001. The measure of the preferential bond orientation in the segment-intrinsic coordinate system, $\langle \tilde{P}_2^{seg}\rangle$, results with the same level of accuracy as $\langle P_2\rangle$ for all segment lengths.[30] However, the measure of preferential segment orientation in the global coordinate system, $\langle P_2^{seg}\rangle$, which is the equivalent of $\langle P_2\rangle$ for segments that contain more than one bond, is computed from a population N^{seg} times smaller than that used in the evaluation of $\langle P_2\rangle$. Therefore, the error bars on $\langle P_2^{seg}\rangle$ are of magnitude $0.001\sqrt{N^{seg}}$. The segment-intrinsic stresses, $\langle {}^{D}\tilde{\sigma}_{ij}{}^{seg}\rangle$, are affected by an error that scales with N^{seg}, i.e., $\pm 0.025\, N^{seg}$ (reducing to the bond-intrinsic stress error for $N^{seg} = 1$).[31] Hence, the most accurate quantity that reflects the internal structure at the segment or chain scale is $\langle \tilde{P}_2^{seg}\rangle$. This is one of the reasons for its extensive use in this analysis.

4. Atomic Level Stress Production in the Bond-Intrinsic Frame

The mechanism of the atomic level stress production in polymeric systems was proposed and discussed in a series of articles.[13−24] The present work builds upon this understanding and extends the formalism (ISF) to larger scales. For completeness, we review here the main conclusions of the previous work.

In ISF, stress is computed based on all bonded and nonbonded interactions in the system (eq 5), in the global and in bond-intrinsic coordinates. One of the fundamental observations in ISF regards the variation of the two stresses in nonequilibrium. It is seen that while the global stress varies significantly during loading and relaxation, the intrinsic stress computed in the bond-intrinsic frame is essentially deformation independent, except for a short period following the cessation of loading. Hence, each bond carries an intrinsic stress which is constant during the α relaxation regime, despite the pronounced preferential bond orientation. The bond-intrinsic stress tensor has a significant deviatoric component due to the effect of the steric shielding. This atomic scale picture of stress production can be related to the system level stress. Each bond-intrinsic frame carries a nonzero deviatoric stress. A random orientation of the bond-intrinsic frames in space leads to an average hydrostatic system level stress. Preferential bond orientation due to system deformation leads to a nonvanishing system level deviatoric stress whose relaxation is related to the randomization of the bond orientation.

This physical picture contradicts the classical entropic spring formulation (ESF) in several fundamental regards. In ISF, the origins of stress are the interactions taking place on the atomic scale, including the excluded volume effect. In ESF, stress is assumed to result from the change in configurational entropy of stretched chains. The global stress computed in ISF results to have primarily an entropic character,[24] in agreement with experimental observations, with no supplementary assumptions being necessary. It is shown in ISF that both bonded and nonbonded interactions are important in stress production, while the ESF neglects the contribution of nonbonded interactions. Furthermore, in ISF the chain backbones are in compression at melt densities, at odds with the assumption made in ESF according to which the chains are always in tension. Finally, since the ESF is based on the scale of a chain, it cannot capture deformation fields varying on the chain scale, while the ISF, which is defined on a smaller scale, has this capability.

The stress relaxation histories and the values of the stress−optical coefficient predicted based on the two formulations are close to each other during the late relaxation period.[32] It is currently unclear whether the predictions become identical at times longer than simulated to date. However, this suggests that the bond-scale description may be extended to the chain scale providing a physical basis for the definition of stress on multiple scales. This motivates the present work.

5. Results

a. **Equilibrium. Intrinsic Stress.** An equilibrium system of chains with $N = 101$ is considered first. The intrinsic stress is evaluated in several segment-intrinsic systems using eq 8 and by considering both bonded and nonbonded interactions. The results are shown in Figure 2 (open symbols). The nonbonded deviatoric stress carried by all segments, $\langle {}^{D}\tilde{\sigma}_{11}^{nb-seg}\rangle$, is positive, while the corresponding stress due to bonded interactions, $\langle {}^{D}\tilde{\sigma}_{11}^{b-seg}\rangle$, is negative and smaller in absolute value. Only one of the normal components of the stress tensor is considered here and in the following discussion because, due to the cylindrical symmetry of all stress tensors considered, the diagonal terms of the deviatoric stress tensor are proportional to each other, while the off-diagonal terms are zero.

Interestingly, the deviatoric stress is scale-invariant. The error bars due to the statistical noise are shown in Figure 2 only on the open symbols. For segments smaller than $N^{seg} = 11$, the error bars are smaller than the size of the symbols. The error increases linearly with N^{seg} and is rather large for $N^{seg} = 101$ (section 3). However, within this accuracy it may be concluded that the end-to-end segment ($N^{seg} = 101$) carries the same deviatoric stress as any other subchain segment. The hydrostatic component of the intrinsic stress does not follow this rule; rather it scales with the number of bonds in the segment.

Figure 3 shows the bonded and nonbonded components of the deviatoric stress computed in the end-to-end intrinsic frame of chains of various length, N. These stresses are essentially independent of chain length. Furthermore, it was shown that the bond-intrinsic stress is chain length independent when computed from

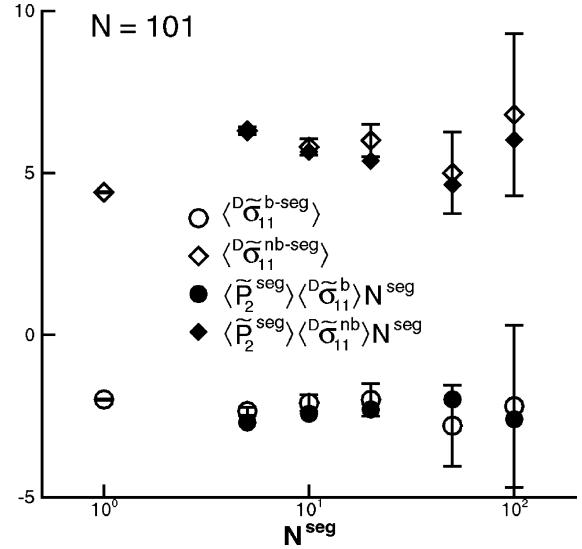

Figure 2. Segment-intrinsic deviatoric stress due to bonded $\langle \tilde{\sigma}_{11}^{b-seg}\rangle$ and nonbonded $\langle \tilde{\sigma}_{11}^{nb-seg}\rangle$ interactions computed in segment-intrinsic coordinates corresponding to chain segments of various length, in the system with $N = 101$. The error bars scale with the length of the segment considered, N^{seg}. For $N^{seg} = 1$ (a bond) they are ± 0.025. The filled symbols correspond to the respective intrinsic stresses evaluated based on eq 9. The error bars on the filled symbols (not shown, for clarity) are of similar magnitude with those on the open symbols. Intrinsic frames defined on various scales carry a scale-invariant deviatoric stress.

chain inner beads.[22] The error bars increase linearly with N, as discussed above.

The segment intrinsic deviatoric stress may be also computed based on the bond-intrinsic stresses and the average bond orientation with respect to the respective segment-scale frame. The procedure parallels that used in[22] to express the global stress in terms of bond-intrinsic quantities. With eqs 6 and 8, the segment-scale intrinsic deviatoric stress reads

$$\langle {}^{D}\tilde{\sigma}_{11}^{seg}\rangle = \frac{2}{3}\left\langle \sum_{k=1}^{N^{seg}} \left[\tilde{t}_{ij}^{k}\, \tilde{a}_{i2}^{k}\, \tilde{a}_{j2}^{k} + \tilde{t}_{ij}^{k}\, \tilde{a}_{i3}^{k}\, \tilde{a}_{j3}^{k} - \frac{\tilde{t}_{ij}^{k}\, \tilde{a}_{i1}^{k}\, \tilde{a}_{j1}^{k}}{2} \right] \right\rangle = N^{seg}\langle [{}^{D}\tilde{\sigma}_{11}^{b} + {}^{D}\tilde{\sigma}_{11}^{nb}]\tilde{P}_2^{seg}\rangle = N^{seg}[\langle {}^{D}\tilde{\sigma}_{11}^{b}\rangle + D\langle {}^{D}\tilde{\sigma}_{11}^{nb}\rangle]\langle \tilde{P}_2^{seg}\rangle \quad (9)$$

The second equality in eq 9 holds under the assumption that the bond-intrinsic stress is a cylindrical tensor. This is exact for $\langle {}^{D}\tilde{\sigma}_{11}^{b}\rangle$, but only approximate for $\langle {}^{D}\tilde{\sigma}_{11}^{nb}\rangle$. In the last equality of eq 9, the average was applied individually on the sum of the bond-intrinsic stresses in parentheses, and on $\tilde{P}_2^{seg}$. This operation can be performed provided the bond-intrinsic stresses and $\tilde{P}_2^{seg}$ are statistically independent. As discussed in ref 22, the separation is not straightforward for the nonbonded component, which is not necessarily a cylindrical tensor locally. The constant D is introduced such to allow the decomposition. The properties of this constant were studied[24] and it was shown that it is chain length and temperature independent, and is a function of density. For the system with $\rho = 1$, D was found numerically to be equal to 2.1.

The segment-intrinsic deviatoric stresses are evaluated with eq 9, based on the bond-intrinsic stresses, $\tilde{P}_2^{seg}$ and by using $D = 2.1$. The results are shown in Figure 2 by filled symbols. Good agreement is seen with

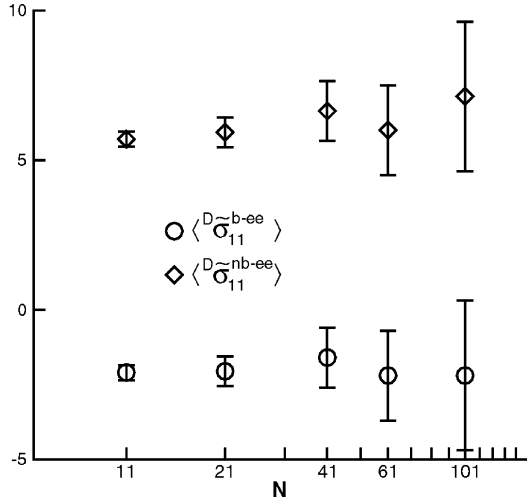

Figure 3. Intrinsic deviatoric stress due to bonded $\langle \tilde{\sigma}_{11}^{b-ee}\rangle$ and nonbonded $\langle \tilde{\sigma}_{11}^{nb-ee}\rangle$ interactions computed in the frame tied to the end-to-end vector as a function of the chain length in various monodisperse systems. The error bars are similar to those in Figure 2.

the segment-intrinsic stresses computed directly from the definition (eq 8). The statistical error affecting the filled symbols (error bar not shown in Figure 2) is of similar magnitude with that of the open symbols; ${}^{D}\tilde{\sigma}_{11}^{b}$, ${}^{D}\tilde{\sigma}_{11}^{nb}$, and $\tilde{P}_2^{seg}$ are rather accurate (see discussion in section 3), but N^{seg} in eq 9 scales the error bars for the segment-intrinsic deviatoric stresses.

This validation of eq 9 suggests that the evaluation of the deviatoric intrinsic stress carried by chain segments reduces to the study of the chain structure described by $\tilde{P}_2^{seg}$ in the segment-intrinsic coordinate system.

The hydrostatic component of the segment-intrinsic stress may be computed as $\langle \tilde{p}^{seg}\rangle = \sum_{k=1}^{N^{seg}} \tilde{p}^{k} = N^{seg}\langle \tilde{p}\rangle$, where $\tilde{p}$ is the hydrostatic component of the (bonded and nonbonded) bond-intrinsic stress. This shows that the segment-intrinsic hydrostatic stress scales with the segment length, as observed in simulations.

Intrinsic Chain Structure. Treloar[33] gives an approximate expression for $\tilde{P}_2^{seg}$ in equilibrium in terms of the end-to-end distance of the segment, r, the bond length, b_0, and the number of bonds in the segment, N^{seg}. The expression was developed for a freely jointed chain using the inverse Langevin formulation and reads

$$\tilde{P}_2^{seg} = \frac{1}{5}\left[3\left(\frac{r}{b_0 N^{seg}}\right)^2 + \left(\frac{r}{b_0 N^{seg}}\right)^4 + \left(\frac{r}{b_0 N^{seg}}\right)^6 \right] \quad (10)$$

Substituting $r = C_\infty b_0 \sqrt{N^{seg}}$ results in

$$\tilde{P}_2^{seg} = \frac{1}{5}\left[3\frac{C_\infty^2}{N^{seg}} + \frac{C_\infty^4}{N^{seg^2}} + \frac{C_\infty^6}{N^{seg^4}} \right] \cong \frac{3}{5}\frac{C_\infty^2}{N^{seg}} \quad (11)$$

For our flexible chains, $C_\infty = 1.15$ and eq 11 becomes $\tilde{P}_2^{seg} \cong 0.7/N^{seg}$ to the first order in N^{seg}. Equations 9 and 11 justify the observed scale invariance (N^{seg} independence) of the segment-intrinsic deviatoric stress shown in Figures 2 and 3.

This relationship applies on the scale of the chain. Figure 4 shows the scaling of $\langle \tilde{P}_2^{ee}\rangle$ and $\langle \tilde{P}_2^{c}\rangle$ with the chain length, N. The dotted line shows the $1/N$ variation. The scaling is followed by both measures of internal

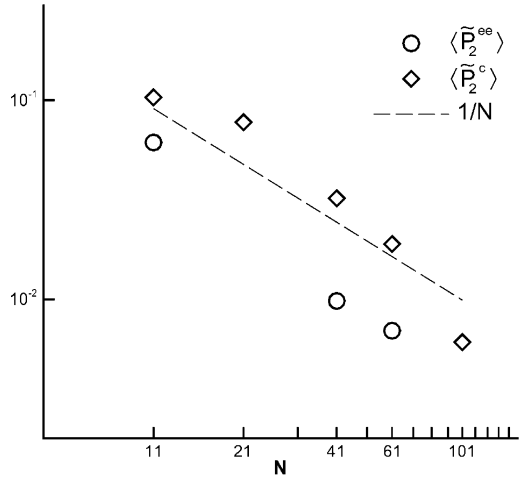

Figure 4. Scaling of the equilibrium intrinsic measure of bond orientation $\tilde{P}_2$ with the chain size in the end-to-end and chain-intrinsic coordinates. The dotted line shows the $1/N$ dependence predicted by eq 11. The error bars are independent of N.

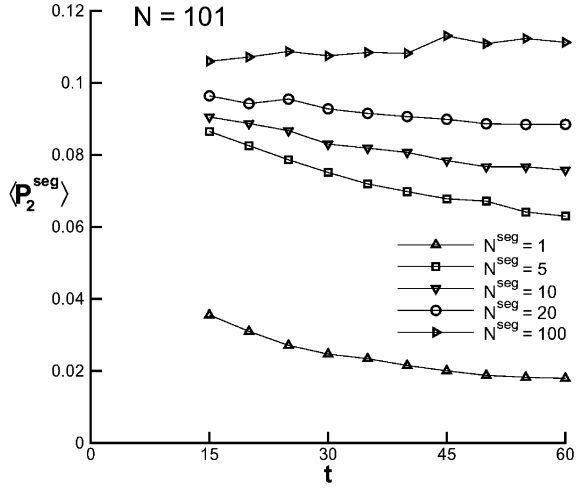

Figure 5. Time variation of the segment preferential orientation in global coordinates during α relaxation for segments of various length in the system with $N = 101$. The error bars scale with $\sqrt{N^{seg}}$, being ± 0.001 for $N^{seg} = 1$ and ± 0.01 for $N^{seg} = 100$.

chain structure, defined in the end-to-end frame and in the chain-intrinsic coordinate system tied to the principal axes of the ellipsoidal coil.

The formulation presented here allows for a connection to be made with the ESF. Equations 9 and 10 define the dependence of the chain-scale deviatoric stress on the end-to-end distance of the chain based on simple topological arguments. With the approximation in eq 11 corresponding to situations in which r is small compared to the fully stretched length of the chain, the chain-scale stress is proportional to the end-to-end distance of the chain. The proportionality constant is expressed in terms of bond-scale intrinsic stresses which are, in turn, temperature dependent. A similar proportionality relationship results in ESF through the standard configuration entropy-based argument. In situations in which r is not a small fraction of the fully extended chain length, the chain-scale stress results from eqs 9 and 10.

Entropic Character of Stress. The chain scale intrinsic stress is assumed to be purely entropic in ESF. Experimentally, the system level stress is largely entropic with a small energetic component (about 10%, depending on the details of the chemistry).[34] In simulations, the system-level global stress is observed to acquire an energetic component at high deformation rates[25] (an effect leading to experimentally observed anomalies in the stress−optical coefficient[35,36]) and at large degrees of chain stretching and alignment.[37] In the present formulation, the deviatoric stress carried by the chain depends exclusively on the bond-scale intrinsic stress (at given structure). It was shown that the two components of the bond-intrinsic stress, due to bonded and nonbonded interactions, are not independently purely entropic.[24] However, their sum has this property, which therefore transfers to the chain scale stress through eq 9. The entropic nature of the atomic level stress is mandated by the important role played by excluded volume interactions in this system of purely repulsive beads.[38]

b. Nonequilibrium. Nonequilibrium systems are considered next. The evolution of the stress and chain structure in intrinsic coordinates is followed during a constant volume elongational deformation of the simulation cell and the subsequent relaxation.

Global stress relaxation was studied in ISF[17,20,22,25] and several relaxation regimes were identified. The structural changes associated with each of these modes were described. During loading, the bonds and chain segments align in the stretch direction and the local environment surrounding a representative bead is distorted. The return to the equilibrium structure of the neighborhood of the representative bead occurs through two fast β relaxation modes. It was previously established by means of simulations that, under the density and temperature conditions of the present study, the β relaxation completes by $t \cong 15$.[25] The duration of the β regime does not depend on the total stretch of the system at given deformation rate. Since the deformation-induced local anisotropy relaxes very fast, a steady-state local structure is reached during loading, even at high deformation rates. Hence, the degree of local anisotropy at the beginning of relaxation is independent of the total stretch of the system. The degree of anisotropy controls the total duration of the β regime, which hence depends only on the deformation rate $\dot{\epsilon}$, on density and temperature. Once the equilibrium local structure of the melt is recovered at the end of the β regime, the subsequent α relaxation entails the return to isotropy of the bond orientation distribution. In what follows, attention is focused on the α relaxation regime during which the bond-intrinsic stresses are constant and equal to the respective quantities in equilibrium.[25]

Global Coordinates. The orientation of the various intrinsic frames with respect to the global coordinate system is defined by $\langle P_2^{seg} \rangle$. During deformation, chain segments of various lengths become preferentially aligned in the stretch direction (Figure 5). The degree of alignment increases with the length of the segment, as expected. This observation is in agreement with SANS data[39] which show different degrees of chain orientation anisotropy on different scales (at various scattering vectors) in a deforming complex fluid. The deformation is essentially affine on large scales, while on smaller scales it is less so, due to the faster relaxation. Similar conclusions are drawn from the data in Figure 5. Useful insight may be gained by analyzing the expected degree of average segment orientation, $\langle P_2^{seg} \rangle$, and average segment length variation during an affine deformation.

The constant volume extensional deformation applied to the system is defined by stretches $\lambda_1 = \lambda$ in the x_1 direction, and $\lambda_2 = \lambda_3 = 1/\sqrt{\lambda}$ in the x_2 and x_3 directions. The segment orientation averaged over the whole system is obtained as

$$\langle P_2^{\text{seg}} \rangle = \frac{1}{2} \times \left[\frac{3}{4\pi} \int_0^{2\pi} \int_0^{\pi} \frac{(\lambda_3 \cos\theta)^2}{(\lambda_1 \sin\theta\cos\varphi)^2 + (\lambda_2 \sin\theta \sin\varphi)^2 + (\lambda_3 \cos\theta)^2} \, d\theta \, d\varphi - 1 \right]$$

$$= \frac{1}{2} \left[\frac{3}{2} \int_0^{\pi} \frac{\lambda^2 \sin\varphi}{\lambda^2 + \frac{\sin^2\varphi}{\lambda}} \, d\varphi - 1 \right] \quad (12)$$

The relative average change in segment length is obtained by following a similar procedure as

$$\left\langle \frac{\Delta r}{r} \right\rangle = \sqrt{\frac{1}{3}\left(\lambda^2 + \frac{2}{\lambda}\right)} - 1 \quad (13)$$

These equations predict a total segment stretch of 1.7% and an orientation of $\langle P_2^{\text{seg}} \rangle = 0.11$ at $\lambda = 1.2$. At $\lambda = 1.5$, the relative segment deformation is 9.2%, and $\langle P_2^{\text{seg}} \rangle = 0.25$. Hence, under relatively small deformations, the average segment does not deform significantly, while its preferential orientation is pronounced.

The data in Figure 5 are in agreement with these predictions. The chain scale ($N^{\text{seg}} = 101$) rotation is essentially affine, with $\langle P_2^{\text{ee}} \rangle \cong 0.105$. Shorter segments are less oriented. The average change in length of the end-to-end vector upon 20% deformation ($\lambda = 1.2$), as imposed here, is computed to be 2% for chains with $N = 101$, 0.75% for $N = 41$, and essentially zero for the shortest chains, $N = 11$. Similar deformations were computed for the large semiaxis of the coils. The deformation of the ellipsoidal coils in the direction of their shorter semiaxes was also evaluated at the end of the loading period. No deformation is visible in these directions in any system considered, within the accuracy of the present calculations.

Chains having their largest semiaxis oriented in the stretch direction deform more than the average, while those at 45° remain essentially undeformed, as required by the imposed affine deformation. However, this observation is not entirely relevant for the present discussion since only the average orientation matters for stress production on the system level.

Mavrantzas and Theodorou performed a similar analysis of the chain deformation in the intrinsic coordinate system tied to the semiaxes of the ellipsoidal coil.[37] They observed that the size of relatively long chains is essentially deformation independent, while shorter chains deform more. As here, both long and short chains rotate significantly in the stretch direction. The apparent discrepancy between their result and our data presumably stems from differences in chain stiffness ($C_\infty = 9.13$, compared to our $C_\infty = 1.15$).

Intrinsic Coordinates. The evolution of the intrinsic stresses on various scales during the α relaxation may be traced by following the time variation of the intrinsic segment-scale structure defined by $\langle \tilde{P}_2^{\text{seg}} \rangle$. As discussed in section 3, $\langle \tilde{P}_2^{\text{seg}} \rangle$ is used to monitor the chain scale structure because the level of statistical noise on this measure is rather low. Figure 6a shows this quantity computed for various segment lengths and in monodisperse systems of various N. Only the α relaxation regime is shown ($t > 15$). The internal structure of the chains is similar in systems of various chain length, a conclusion drawn above in connection with Figure 3 for a system in equilibrium. Furthermore, $\langle \tilde{P}_2^{\text{seg}} \rangle$ for short segments ($N^{\text{seg}} = 5$, 10, and 20) does not change significantly from its equilibrium value during deformation. These segments appear to rotate without stretching. Slightly more pronounced distortion is observed for longer segments, e.g., for $N^{\text{seg}} = 101$.

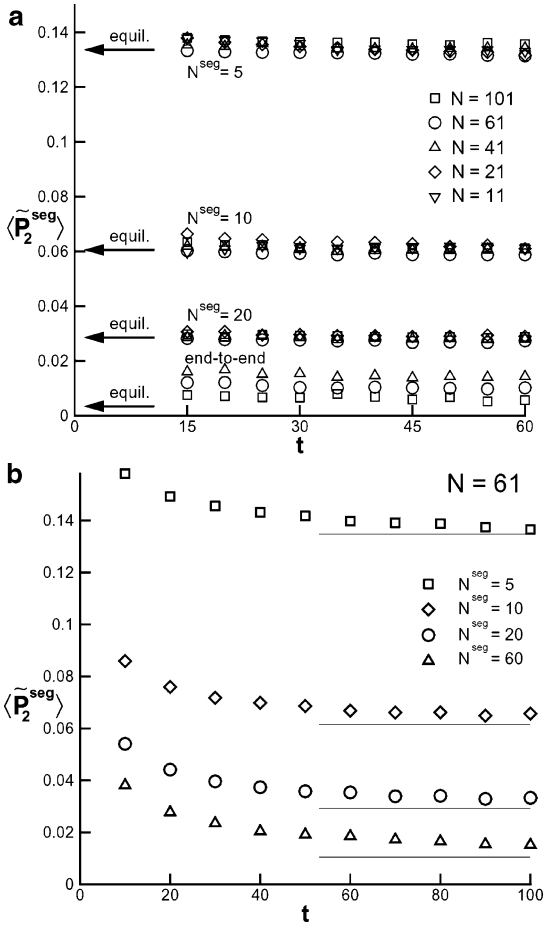

Figure 6. Time variation of the intrinsic measure of preferential bond orientation during system relaxation following a constant volume elongation, for segments of various length in systems of $N = 11$, 21, 41, 61, and 101 beads per chain. In part a the system relaxes after 20% elongational deformation of the simulation cell (α relaxation only). The internal structure of the chains is weakly perturbed compared to the equilibrium configuration. The similar quantity corresponding to the system deformed by 50% is shown in part b. The internal structure of the chains departs significantly from equilibrium in this case. Equilibrium values are indicated by horizontal lines in part b and by arrows in part a. The statistical error affecting these quantities is independent of N and N^{seg} and the bars are smaller than the size of the symbols.

This observation has implications for the time variation of the segment-intrinsic stress. This quantity may be evaluated for segments of various lengths using eq 9 and based on the bond-intrinsic stress and $\langle \tilde{P}_2^{\text{seg}} \rangle$. The bond-intrinsic stress is deformation insensitive during the α regime[20,22,25] and hence, the only time dependence of $\langle {}^D\tilde{\sigma}_{11}^{\text{seg}} \rangle$ is due to $\langle \tilde{P}_2^{\text{seg}} \rangle$. The data in Figure 6a suggest that the deviatoric stress carried by short segments is essentially deformation independent during this relax-

ation regime. The stress carried by longer segments is not deformation independent. Its return to equilibrium is associated with the relaxation of the smaller length scale structure of the chain through the fast Rouse modes. The equilibrium values for $\langle \tilde{P}_2^{seg} \rangle$ obtained here (shown by arrows in Figure 6a) are identical to those found in[40] for equivalent segment lengths.

This situation is better represented in Figure 6b, which shows the same quantities in a system deformed up to 50% ($\lambda = 1.5$) under similar rate, density and temperature conditions. The β relaxation regime ends at about $t \cong 15$, time at which both the orientation and the average segment (chain) size are significantly different than in equilibrium. The equilibrium $\langle \tilde{P}_2^{seg} \rangle$ values are shown by horizontal continuous lines in the figure. The segment internal structure returns to isotropy at a rate dependent on the segment length. The structure of the segment $N^{seg} = 5$ reaches equilibrium by $t \sim 90$, while the chain scale structure ($N^{seg} = 60$) is still out of equilibrium at that time.

Further insight into the relaxation rate of the internal segment (chain) structure compared to the rate of segment (chain) rotation in global coordinates may be obtained by replotting the data in Figure 6a after proper normalization.

Figure 7 shows results for systems of chain with $N = 11$, $N = 41$, and $N = 101$. The time variation during α relaxation of three functions is shown: the orientation of the large semiaxis of the ellipsoidal chains in global coordinates, $\langle P_2^c \rangle$, the length of the large semiaxis of the coils, $\langle c_1 \rangle$, and the departure from equilibrium of the chain structure in chain-intrinsic coordinates, $\langle \tilde{P}_2^c \rangle$. The first measure describes the rotation of the chain in global coordinates, while the last two measures represent the evolution of the internal chain structure. All quantities are normalized by their value at the beginning of the α relaxation regime ($t = 15$). We note that similar results are obtained in the segment-intrinsic coordinate system tied to the chain end-to-end vector.

Figure 7a shows results for the short chain, $N = 11$. The internal structure of these chains does not depart from equilibrium during deformation and the chain carries a deformation insensitive intrinsic stress. However, the chains rotate in global coordinates approximately as rigid objects. This is possible since $N = 11$ is below the entanglement length which, in this model, is estimated to be about $N = 35$.[41] Mondello and Grest[42] also observe that short chains retain a significant degree of rigidity during melt shearing. Their rigid chains having $N = 64$ correspond approximately to our flexible chains with $N = 15$. In their simulation, the chains are seen to rotate rigidly after time $t = 10$ ps, far before full relaxation of the system is achieved.

The situation is different in the long chain system with $N = 101$ in which chains both rotate and distort during deformation (Figure 7c). The internal chain structure and the overall chain orientation return to equilibrium with different rates. The normalized $\langle \tilde{P}_2^c \rangle$ decays much faster than $\langle P_2^c \rangle$. First the chains tend to recover their internal equilibrium structure and then rotate in order to randomize their orientation. This may be understood based on the Rouse description of chain dynamics. In absence of coupling between modes, a large fraction of the total relaxation time is spent after the second slowest Rouse mode has decayed and before the completion of the relaxation due to the slowest mode.

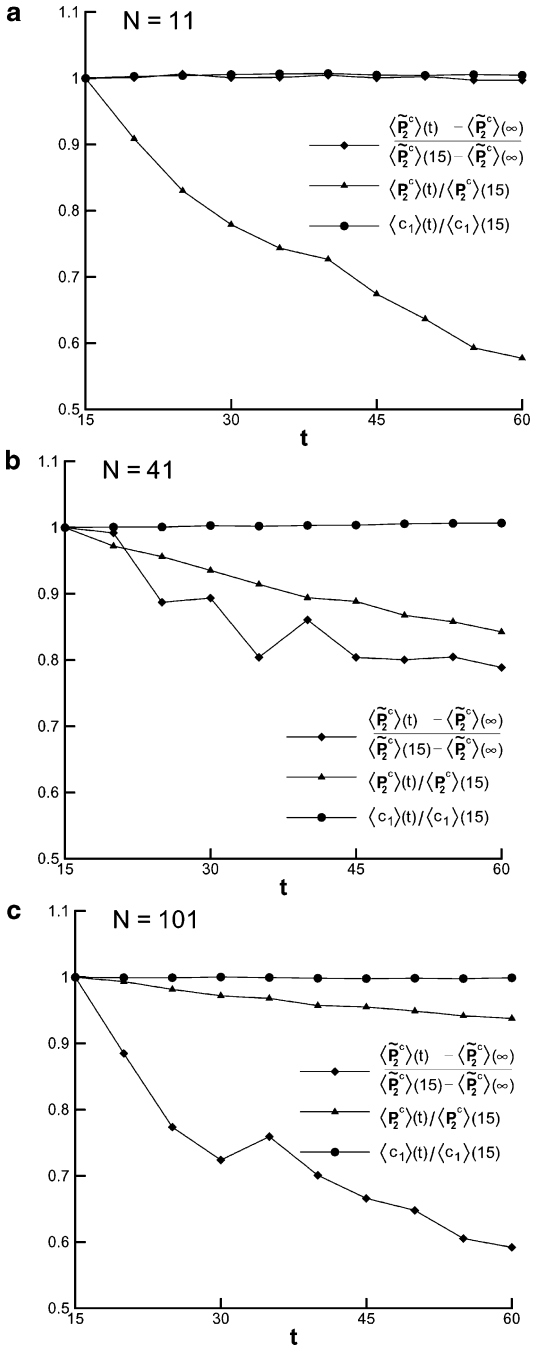

Figure 7. Time variation of various measures of the chain structure and global chain orientation during the α relaxation regime following an elongational deformation of the system by 20%. Results for systems of $N = 11$ (a), $N = 41$ (b), and $N = 101$ (c) are shown. The chain size characterized here by $\langle c_1 \rangle$ is seen to relax very little during this period, whereas the internal chain structure defined by $\tilde{P}_2^c$ changes significantly (for $N = 41$ and 101). The size and internal structure of the shortest chain (a) are not perturbed during deformation and therefore do not relax. The percentage relaxation of $\tilde{P}_2^c$ is larger the longer the chains. Chains are aligned in the stretch direction during deformation. Their return to the random orientation is slower as the chain length increases. It appears that in short chain systems relaxation is mainly associated with the rotation of the coils in global coordinates. Long chains deform and rotate during loading and relax through two modes: the faster mode is associated with the return to isotropy of the internal structure of the chain (described by $\tilde{P}_2^c$), while the second is due to the overall chain rotation in global coordinates. The crossover from short chain to long chain behavior corresponds to $N \cong 30$ (c), which is approximately the entanglement length in these systems.

As discussed, $\langle c_1 \rangle$ does not depart significantly from equilibrium. However, its relaxation rate is low, much smaller than that of $\langle \tilde{P}_2^c \rangle$. On the other hand, eq 10 predicts a direct correlation of the end-to-end vector length with $\langle \tilde{P}_2^c \rangle$ and, based on this equilibrium physical picture, the two rates should be similar. This seems not to be the case in nonequilibrium. Furthermore, it results that it is possible to have a high degree of bond alignment within the coil, with relatively little overall coil deformation (characterized by the semiaxes of the coil). The pronounced orientation on all scales is due to the tendency of the system to follow an affine deformation during loading. A similar effect was observed by Sotta et al.[43] for short probe chains dissolved in a stretched network of longer chains.

Figure 7b shows the same quantities in a system with $N = 41$. The relaxation rate of the internal chain structure is similar to that of chain rotation in global coordinates. Hence, the data suggest that a crossover from a situation dominated by chain rotation to one dominated, at early times, by chain internal structure relaxation (chain size variation) occurs at about $N \sim 30$ (extrapolated based on Figure 7). The crossover corresponds to the entanglement length in this model.

These observations are in agreement with published results obtained using other polymer models and different simulation procedures. Haramandaris et al.[44] use a hierarchical method to evolve a model polymeric system that includes bending and torsional potentials. The system of chains is generated in its deformed (oriented) state and is relaxed by molecular dynamics in a modified ensemble. The time variation of the stress, the chain end-to-end vector length and a measure equivalent to our $\langle P_2^{ee} \rangle$ is computed in two polydisperse systems having average chain length of $N = 24$ and $N = 78$. The end-to-end vector length is seen to return to its equilibrium value faster than $\langle P_2^{ee} \rangle$. The difference in relaxation rates increases with the chain length. Importantly, the global deviatoric stress follows the dynamics of $\langle P_2^{ee} \rangle$.

Similar results are obtained by Mondello and Grest[42] in short alkanes. They observe that the global and the local backbone orientation track each other after a nonexponential transient. The time at which the molecules seem to rotate as rigid blocks (end of the first nonexponential regime) depends strongly on chain length, as expected.

Barsky and Slater[45] performed MD simulations of bidisperse systems of small and long chain polymers in an effort to expand upon the experimental observations of Sotta et al.[43] In a system of predominantly long chains relaxing after an elongational deformation, they observe the length of the end-to-end vector of short chains to recover much faster than their orientational order parameter. Since the short probe chains are below the entanglement length, their orientation couples through the excluded volume effect to that of neighboring long chains, presumably probing the behavior of sub-segments of the host chains. This behavior is consistent with the present results and with experimental data.[43,46]

It is interesting to observe that the behavior described here in nonequilibrium may be qualitatively associated with the equilibrium behavior of chains in the vicinity of a flat impenetrable surface. In the flat surface case and in the presence of weak and moderate attractive interactions between the polymer and the wall, the ellipsoidal chains do not deform, rather rotate with their large semiaxis in the direction tangential to the interface: a "docking" transition.[47] Hence, the chains are highly oriented in a thin layer at the wall, whereas in the bulk they are randomly oriented in space. This behavior may be understood based on the observation that chain deformation entails a larger penalty in free energy compared to that associated with chain rotation.

In nonequilibrium, as long as the deformation compatibility condition is fulfilled by simple chain rotation, this will be the preferred deformation mode over chain distortion. Similarly, during relaxation after pronounced system deformation, the distorted and rotated chains should (within the limits of coupling between relaxation modes) rebound first to their equilibrium internal configuration and then collectively reorient, as observed in the present study.

Global Stress. The global deviatoric stress may be computed using eqs 5 and 6, or based on the rotation of the bond-intrinsic stress (eq 7) in global coordinates (σ_{or} in refs 22 and 25). The two procedures lead to identical results during the α relaxation regime,[32] once the bond-intrinsic stress has recovered its equilibrium value. The global deviatoric stress written as a function of the deviatoric intrinsic stresses (bonded and nonbonded) reads[22]

$$\langle {}^D\sigma_{11} \rangle = [\rho_b \langle {}^D\tilde{\sigma}_{11}^b \rangle + \rho_a D \langle {}^D\tilde{\sigma}_{11}^{nb} \rangle] \langle P_2 \rangle \qquad (14)$$

where ρ_b and ρ_a are the bond and atom (bead) number densities, $D = 2.1$ and $\langle P_2 \rangle$ is the average measure of bond orientation in global coordinates. The quantity in parentheses in eq 14 is the inverse of the stress−optical coefficient.

The global stress may be also obtained by a rotation from the segment (or chain)-intrinsic coordinate system to the global coordinates. As long as the segment-intrinsic stress (including bonded and nonbonded contributions), $\langle {}^D\tilde{\sigma}_{11}^{seg} \rangle$, is a cylindrical tensor, it is possible to write:

$$\langle {}^D\sigma_{11} \rangle = \rho^{seg} \langle \langle {}^D\tilde{\sigma}_{11}^{seg} \rangle P_2^{seg} \rangle = \rho \langle \langle [{}^D\tilde{\sigma}_{11}^b + {}^D\tilde{\sigma}_{11}^{nb}] \tilde{P}_2^{seg} \rangle P_2^{seg} \rangle \qquad (15)$$

where the bond and atom (bead) number densities were taken to be equal to the system density, ρ. Under restrictive conditions eq 15 may be simplified to

$$\langle {}^D\sigma_{11} \rangle = \rho \langle {}^D\tilde{\sigma}_{11}^b + D {}^D\tilde{\sigma}_{11}^{nb} \rangle \langle \tilde{P}_2^{seg} \rangle \langle P_2^{seg} \rangle \qquad (16)$$

The structure of the chain segment defined by $\langle \tilde{P}_2^{seg} \rangle$ has to be independent of the bond-intrinsic stress. This condition is similar to that required for the separation of $\langle P_2 \rangle$ in eq 14 and is immediately fulfilled, since bond-intrinsic stresses are deformation insensitive during the α relaxation regime ($t > 15$).[22] Once this is fulfilled, the bond-intrinsic stresses are statistically independent of the segment orientation in global coordinates.

The more restrictive condition required by the separation in eq 16 is the statistical independence of $\tilde{P}_2^{seg}$ and P_2^{seg}, which is achieved only once the internal segment (chains) structure returns to equilibrium. Under these conditions, the global deviatoric stress may be computed based on eq 14 or eq 16. These two equations extend the validity of the ISF picture of stress production from the bond to the segment and chain scale. In conditions in which eq 16 is valid, the global stress results due to the preferential orientation of

chains (subchain segments) which have the equilibrium internal structure and therefore rotate as "rigid entities." Such structures carry a deformation insensitive intrinsic deviatoric stress. Full system equilibration results when the chain orientation becomes random. We note that this definition of stress is valid for any chain or segment length larger than the persistence length. When such conditions exist, eqs 14 and 16 lead to

$$\frac{\langle P_2 \rangle}{\langle P_2^{\text{seg}} \rangle} = \langle \tilde{P}_2^{\text{seg}} \rangle \tag{17}$$

where $\langle \tilde{P}_2^{\text{seg}} \rangle$ is a quantity that may be obtained from equilibrium simulations (Figures 4 and 6a). This equation was conjectured to be valid and used in ref 40.

Finally, we turn to the conditions that need to be fulfilled for the physical picture described above to apply. As stated, the separation in eq 16 is valid only once the internal structure of the chain has returned to equilibrium, while the chain orientation distribution function did not yet reach spatial uniformity. Although the data in Figure 7 show that, for long chains, the internal chain structure equilibrates faster than the global chain orientation, the simulations are too short to fully support the mechanism proposed here.

However, full support is provided by the much longer simulations of a similar model performed by Faller et al.[48] They consider a chain with $N = 200$, much longer than the entanglement length, and observe that both the global stress and $\langle \tilde{P}_2^{\text{seg}} \rangle$ decay following two regimes. The first is described by a power law while the second is exponential. Once the exponential regime is reached, the ratio in eq 17 becomes a constant, i.e., the exponentials corresponding to various segment lengths have the same relaxation time, but different preexponential factors. Their results have been validated by double-quantum NMR experiments.[48]

This observation is also in agreement with the conclusions of Mondello and Grest,[42] although Faller et al.[48] consider much longer chains than Mondello and Grest. The ratios ($\langle P_2 \rangle / \langle P_2^{\text{seg}} \rangle$) of Faller et al. cannot be compared directly with $\langle \tilde{P}_2^{\text{seg}} \rangle$ in Figure 4 (eq 17) because their results are for chains much stiffer than those considered here. Stiff chains are known to behave slightly differently than fully flexible chains even after chain length renormalization. Nevertheless, their data support the physical picture described in this report.

6. Conclusions

A physical description of stress production that unifies the bond, segment and the chain scales within the intrinsic stress framework is proposed. The stress is produced by bonded and nonbonded interatomic interactions on the scale of a bead. The global, system level stress results by averaging the atomic level stress in global coordinates. The atomic level stress may be also computed in a family of mobile frames tied to the generic bond, to the generic chain segment, or to the representative ellipsoidal coil. These intrinsic stresses have significant deviatoric components. It is shown that the bond, the chain segment, and the whole chain carry the same deviatoric stress. The hydrostatic component of the intrinsic stress scales with the segment length.

The scale invariance of the deviatoric intrinsic stress allows for the development of a unitary description of stress production. In ISF, the global deviatoric stress is seen as being generated by the preferential orientation of bond-intrinsic frames each carrying a nonzero deviatoric intrinsic stress which, in turn, is independent of melt deformation. This physical picture is translated to larger scales by showing that the global deviatoric stress can be similarly viewed as being associated with the preferential orientation of larger units (segments or chains) which carry a nonzero deviatoric stress. The extension is valid provided the intrinsic stress computed on larger scales (segments or chains) is deformation insensitive. This situation exists late in the relaxation history.

It is shown that the reorientation of segments (and chains) during the α relaxation regime is described by two processes that take place with different rates. The fast mode is associated with the return of the internal chain structure to the equilibrium configuration. Faller et al.[48] observed this nonexponential relaxation regime but did not associate a physical interpretation to it. Once the internal chain configuration (the size of the ellipsoidal coil *and* the orientation of bonds with respect to the coil axis) has equilibrated, the chains rotate to randomize the chain orientation in the global coordinate system. The collective rotation of the chains is described by an exponential decay.[42,48] Once the first regime completes, the chain scale intrinsic stress reaches the equilibrium value. The physical picture of global stress production described here applies to this second regime.

Acknowledgment. This work was supported by the US National Science Foundation through Grant CMS-9908025.

References and Notes

(1) Guth, E.; Mark, H. *Monatsh. Chem.* **1934**, *65*, 93.
(2) Fukuda, T.; Takada, A.; Miyamoto, T. *Macromolecules* **1991**, *24*, 6210.
(3) Fukuda, T.; Kawabata, K.; Tsujii, Y.; Miyamoto, T. *Macromolecules* **1992**, *25*, 2196.
(4) Kroger, M.; Luap, C.; Muller, R. *Macromolecules* **1997**, *30*, 526.
(5) Ronca, G.; Allegra, G. *J. Chem. Phys.* **1975**, *63*, 4990.
(6) Flory, P. J.; Erman, B. *Macromolecules* **1982**, *15*, 800.
(7) Edwards, S. F. *Proc. Phys. Soc. London* **1967**, *92*, 9.
(8) De Gennes, P. G. *J. Phys., Lett.* **1974**, *35*, L-133.
(9) Marucci, G. *Macromolecules* **1981**, *14*, 434.
(10) Erman, B.; Flory, P. J. *Macromolecules* **1982**, *15*, 806.
(11) Doi, M.; Edward, S. F. *J. Chem. Soc., Faraday Trans.* **1978**, *74*, 1802.
(12) Sahouani, H.; Lodge, T. P. *Macromolecules* **1992**, *25*, 5632.
(13) Gao, J.; Weiner, J. H. *J. Chem. Phys.* **1989**, *90*, 6749.
(14) Gao, J.; Weiner, J. H. *Macromolecules* **1991**, *24*, 5179.
(15) Gao, J.; Weiner, J. H. *Macromolecules* **1992**, *25*, 3462.
(16) Gao, J.; Weiner, J. H. *J. Chem. Phys.* **1993**, *98*, 8256.
(17) Gao, J.; Weiner, J. H. *Macromolecules* **1994**, *27*, 1201.
(18) Gao, J.; Weiner, J. H. *Science* **1994**, *266*, 748.
(19) Gao, J.; Weiner, J. H. *J. Chem. Phys.* **1994**, *100*, 682.
(20) Gao, J.; Weiner, J. H. *Macromolecules* **1996**, *29*, 6048.
(21) Picu, R. C.; Weiner, J. H. *J. Chem. Phys.* **1998**, *108*, 4984.
(22) Picu, R. C.; Loriot, G.; Weiner, J. H. *J. Chem. Phys.* **1999**, *110*, 4678.
(23) Picu, R. C. *Macromolecules* **1999**, *32*, 7319.
(24) Picu, R. C. *Macromolecules* **2001**, *34*, 5023.
(25) Picu, R. C.; Pavel, M. C. *Macromolecules* **2002**, *35*, 1840.
(26) Ozmusul, M. S.; Picu, R. C. *Polymer* **2002**, *43*, 4657.
(27) Berendsen, H.; Postma, J.; van Gunsteren, W. *J. Chem. Phys.* **1984**, *81*, 3684.
(28) Cannon, J. W.; Aronovitz, J. A.; Goldbart, P. *J. Phys.* **1991**, *1*, 629.
(29) Janszen, H. W. H. M.; Tervoort, P. A.; Cifra, P. *Macromolecules* **1996**, *29*, 5678.
(30) The measure of the average bond orientation in global coordinates is computed as $\langle P_2 \rangle = (1/NN_c) \sum_{k=1}^{NN_c} P_2(\theta_k)$, while the measure of preferential bond orientation with respect to

the $\tilde{x}_1^{seg}$ axis is evaluated as $\langle \tilde{P}_2^{seg} \rangle = \sum_{l=1}^{NN_c/N^{seg}} [(1/N^{seg}) \sum_{k=1}^{N^{seg}} \tilde{P}_2(\tilde{\theta}_k^1)](N^{seg}/NN_c) = (1/NN_c) \sum_{l,k} \tilde{P}_2(\tilde{\theta}_k^1)$ (see the discussion related to eq 4). Therefore, the two measures are affected by the same level of statistical noise.

(31) The bond-intrinsic stresses are evaluated as $\langle {}^D\tilde{\sigma}_{ij}^b \rangle = (1/NN_c) \sum_{k=1}^{NN_c} {}^D\tilde{\sigma}_{ij_k}$, while the segment intrinsic deviatoric stress results from the average $\langle {}^D\tilde{\sigma}_{ij}^{seg} \rangle = \sum_{l=1}^{NN_c/N^{seg}} [\sum_{k=1}^{N^{seg}} {}^D\tilde{\sigma}_{ij}(\tilde{\theta}_k^1)] \cdot (N^{seg}/NN_c) = N^{seg}[(1/NN_c)\sum_{l,k} {}^D\tilde{\sigma}_{ij}(\tilde{\theta}_k^1)]$ (see the discussion related to eq 8). Therefore, the segment-intrinsic stress carries a statistical noise N^{seg} times larger than that affecting the bond-intrinsic stress.

(32) Loriot, G.; Weiner, J. H. *J. Polym. Sci.* **1998**, *B45*, 143.

(33) Treloar, L. R. G. *Trans. Faraday Soc.* **1954**, *50*, 881.

(34) Treloar, L. R. G. *The physics of rubber elasticity*; Clarendon: Oxford, England, 1975.

(35) Inoue, T.; Okamoto, H.; Osaki, K. *Macromolecules* **1991**, *24*, 5670.

(36) Inoue, T.; Uematsu, T.; Osaki, K. *Macromolecules* **2002**, *35*, 820.

(37) Mavrantzas, V. G.; Theodorou, D. N. *Macromolecules* **1998**, *31*, 6310.

(38) Weiner, J. H. *Statistical mechanics of elasticity*; Dover: New York, 2002; p A31.

(39) Muller, R.; Pesce, J. J.; Picot, C. *Macromolecules* **1993**, *26*, 4356.

(40) Taylor, D. J. R.; Stepto, R. F. T.; Jones, R. A.; Ward, I. M. *Macromolecules* **1999**, *32*, 1978.

(41) Kremer, K.; Grest, G. *J. Chem. Phys.* **1990**, *92*, 5057.

(42) Mondello, M.; Grest, G. *J. Chem. Phys.* **1995**, *103*, 7156.

(43) Sotta, P.; Deloche, B.; Herz, J.; Lapp, A.; Durand, D.; Rebadeux, J. C. *Macromolecules* **1987**, *20*, 2769.

(44) Haramandaris, V. A.; Mavrantzas, V. G.; Theodorou, D. N. *Macromolecules* **2000**, *33*, 8062.

(45) Barsky, S.; Slater, G. W. *Macromolecules* **1999**, *32*, 6348.

(46) Brereton, M. G. *Macromolecules* **1993**, *26*, 1152.

(47) Pakula, T. *J. Chem. Phys.* **1991**, *95*, 4685.

(48) Faller, R.; Muller-Plathe, F.; Heuer, A. *Macromolecules* **2000**, *33*, 6602.

MA0259867